Monte Carlo Simulations of Dendrimer−Polymer Conjugates

Tong Zhou and Shing Bor Chen*

Department of Chemical and Biomolecular Engineering, National University of Singapore, Singapore 117576

Received May 13, 2005; Revised Manuscript Received August 1, 2005

ABSTRACT: Conformational properties of a neutral dendrimer−polymer conjugate are investigated by off-lattice Monte Carlo simulations in near Θ condition. The conjugate is a dendrimer with linear polymers grafted to its end segments. A bead−spring model along with Lennard-Jones potential is applied to simulate the structure of the conjugates. Also investigated are dendrimers without polymer attachment up to seven generations for comparison. It is found that the grafted polymers can expand the dendrimer moiety of a conjugate owing to the additional steric effect imposed. As a result, the core dendrimer has a more ordered structure and its terminal segments fold back to a lesser extent. Nevertheless, no clear boundary separates the dendrimer moiety and the polymer attachment. The grafted polymers with sufficient length show a scaling behavior of brushlike chains, and hence the conjugate is less compact than an unmodified dendrimer. The dendrimer swelling caused by the polymer attachment gives rise to more free space for drug encapsulation. The size expansion increases with the length of grafted chains until it gets saturated when the chain becomes sufficiently long.

1. Introduction

Dendrimers are special synthetic macromolecules with regular branches showing a cascade topology. These treelike polymers have recently found many applications[1−3] due to their well-defined structure, low polydispersity, and small hydrodynamic radii in comparison to other polymers of comparable molecular weight. Dendrimers are synthesized by the convergent or divergent repetition of a reaction sequence, which was once thought to produce a dense shell consisting of terminal groups and a loose core. It has been known that guest molecules can penetrate into a dendrimer and become entrapped thanks to physical hindrance[4,5] or chemical bonding.[6,7] The encapsulation ability allows dendrimers to serve as potential drug carriers. To be used as drug carriers in vivo, however, dendrimers must fulfill some essential biological demands, such as nontoxicity, nonimmunogenicity, biocompatibility, and selectivity. Cationic macromolecules have been known to cause destabilization of cell membranes, leading to cell lysis.[8] Therefore, dendrimers with cationic terminal groups, such as the widely used and well-characterized amino-terminated polyamidoamine (PAMAM), are quite cytotoxic and unable to stay in circulation for the time needed to have a clinical effect.[9,10]

To improve the biological application of PAMAM dendrimer, scientists have attempted to graft poly(ethylene glycol) (PEG), which is a nontoxic and nonimmunogenic water-soluble polymer, to the terminal groups of the dendrimer by covalent bonding.[11] By this means, the dendrimer−polymer conjugate has a lower cytotoxicity and good biocompatibility due to its hydrophilic shell consisting of PEG. Also, its encapsulation capability can be enhanced for anticancer drugs; Kojima et al.[7] reported that the PAMAM (four generations) with attached poly(ethylene glycol) monomethyl ether (M-PEG, $M_w = 2000$ g/mol) encapsulated around 4 times the amount of adriamycin and 1.5 times that of methotrexate as the corresponding unmodified PAMAM did. This enhancement in encapsulation was speculated to be due in part to an increase in the free space of the dendrimer moiety. This interesting experimental observation motivates us to conduct the present simulation study to investigate the effect of grafted linear polymers on the structural behavior of the surrounded dendrimer.

For the past two decades, the structural and dynamic behaviors of dendrimers have been extensively investigated. The pioneering work of de Gennes and Hervet[12] based on a self-consistent mean-field analysis predicted the dendrimer size to scale as $N^{1/5}P^{2/5}$, where N is the number of monomers and P is the spacer length. Their theory also found that a dendrimer consists of a dense shell and a loose core. Since then, numerous studies have been conducted to verify their findings by small-angle neutron and X-ray scattering experiments[13−15] as well as by Monte Carlo (MC), molecular dynamics (MD), and Brownian dynamics (BD) simulations.[16−35] Controversially, many works[17,24,29,30,34] obtained an approximately $N^{1/3}$ dependence of dendrimer size rather than $N^{1/5}$. Moreover, the monomer density distribution function was found to be higher in the inner region than in the outer, indicating that the shell is not as dense as thought previously. The controversy in the scaling behavior of dendrimer size indeed arises from the fact of not large enough N. Sheng et al.[23] applied the Flory theory and off-lattice MC simulations to find that the dendrimer size scales as $N^{1/5}P^{2/5}(G + 1)^{2/5}$ in a good solvent and $N^{1/3}$ in a poor solvent, where G is the generations of the dendrimer. Since $G \sim \ln N$, the size in a good solvent is accordingly in proportion to $N^{1/5}(\ln N)^{2/5}$, which coincidentally can also be acceptably fitted by $N^{1/3}$ in a double-log plot for not so large N, a limitation in many simulation works. For the Θ condition, Giupponi and Buzza[35] recently followed the same approach but included three-body interactions to obtain the scaling $N^{1/4}P^{1/4}(G + 1)^{1/4}$, which was supported by their lattice MC simulations.

Simulation studies have reported that a dendrimer of high generation essentially has a shape close to a

* To whom all correspondence should be addressed. E-mail: checsb@nus.edu.sg.

10.1021/ma050997w CCC: $30.25
Published on Web 08/27/2005

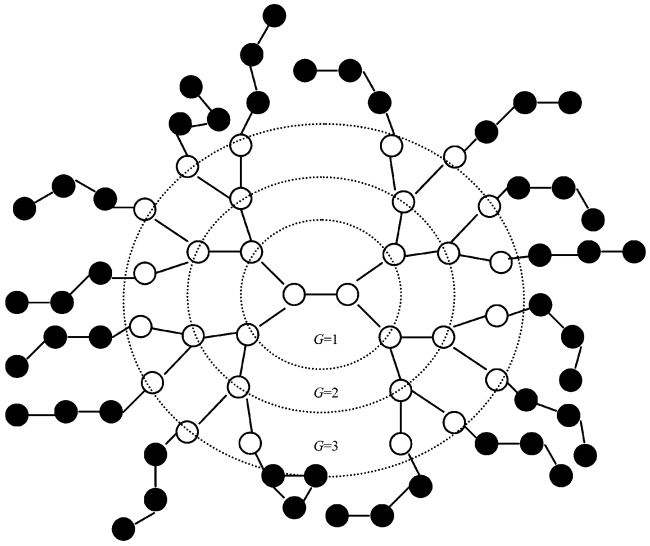

Figure 1. Schematic diagram of a G3 dendrimer−polymer (16 3-mers) conjugate.

sphere.[25,29] For PAMAM, Maiti et al.[29] conducted MD simulations at the atomistic level only in a gas phase (without solvent) because the detail of atomistic structure of a dendrimer molecule has already rendered the computation very intensive. They found that the aspect ratios of a dendrimer decrease from 1 to 6 generations and then increase slightly at higher generations due to dramatically increased steric constrain. Terminal groups of a dendrimer with higher generations are found to be able to fold back and penetrate into its interior, therefore reducing the inner space for encapsulation of guest molecules.[17,29] Moreover, some drugs are reported to be only able to bind with the surface groups;[36] thus, the back-folding of the terminal groups also reduces a dendrimer's ability to entrap these drugs. It is worth pointing out that the scaling behavior and qualitative structural features predicted by the atomistic-level simulations[29] can indeed be captured by less demanding coarse-grained simulations,[16,17,23,24,32] in which the solvent is treated as a continuum and its effect (i.e., solvent quality) can be changed by varying interaction parameters.

Although the structural properties of dendrimers have been extensively studied, there exists no simulation study on the effect of grafted polymers on their behavior, to our best knowledge. In view of the practical applicability and advantage of dendrimer−polymer conjugates in drug encapsulation, it is important to gain a fundamental understanding of their structure. The present study aims to investigate the effects of attached linear polymers on the size and shape of the dendrimer moiety of a conjugate, and the monomer distribution by coarse-grained off-lattice Monte Carlo simulations, in an attempt to explain the experimentally observed enhancement in drug encapsulation using such conjugates.

2. Model and Simulation

We consider a dendrimer−polymer conjugate, for which linear polymer chains (filled circles) are attached to the dendrimer (open circles) as shown in Figure 1. The architecture adopted here is a dendron emanating from two central connected trifunctional units (zeroth generation),[7,25,26,29,30,32,35] rather than one emanating from a single central monomer that is also commonly seen in the literature.[17,18,21−23,27,28,33,34] The bonded spherical beads of the same mass are utilized to represent the monomers of the dendrimer and of the linear polymers by assuming the spacer length to be unity. The bonding energy is modeled by the energy of a harmonic spring:

$$U^{\mathrm{S}} = k(r - l_0)^2 \tag{1}$$

with k being the spring constant, l_0 the equilibrium bond length, and r the distance between two bonded beads. In this study, the spring constant k is set to be $200k_{\mathrm{B}}T/l_0^2$ to render the bond length fluctuation within 5% of l_0, where k_{B} is the Boltzmann constant and T is the absolute temperature. The interaction between nonbonded beads is described by a Lennard-Jones (LJ) potential:

$$U^{\mathrm{LJ}} = 4w\left[\left(\frac{\sigma}{r}\right)^{12} - \left(\frac{\sigma}{r}\right)^{6}\right] \tag{2}$$

Using (2), the solvent quality is determined by the values of w and cutoff r_{cut}. We specify $\sigma = 0.8l_0$, $w = 0.3k_{\mathrm{B}}T$, and $r_{\mathrm{cut}} = 2.5\sigma$ as in the study of Rey et al.[16] Using these parameters, our test on free linear polymers finds that their radius of gyration follows a power law with an exponent of about 0.52, thereby corresponding to a state near the Θ condition.

The total number of beads N in the dendrimer relates to its terminal generation G by the following equation

$$N = 2^{G+2} - 2 \tag{3}$$

and the number of end beads N_{end} is

$$N_{\mathrm{end}} = 2^{G+1} \tag{4}$$

We assume that each of the end beads is attached by a linear chain of N_{chain} bonded beads. Therefore, the total number of beads in the dendrimer−polymer conjugate is

$$N_{\mathrm{total}} = N + N_{\mathrm{end}}N_{\mathrm{chain}} \tag{5}$$

For dendrimers without attached chains, we investigate the cases of G ranging from 2 to 7, corresponding to N from 14 to 510. For dendrimer−polymer conjugates, we fix $G = 3$ in most of the cases and vary the length of the attached chains from $N_{\mathrm{chain}} = 2$ to 30, which corresponds to N_{total} between 62 and 510.

Hereafter, we nondimensionalize all the lengths by l_0 and energy by $k_{\mathrm{B}}T$. Off-lattice MC simulation with the standard Metropolis algorithm[37] is used. The configuration is changed by a trial move of a randomly selected bead in a spherical region of radius 0.3 The Metropolis criterion, $\Delta E \leq -\ln W$, where ΔE is the energy change from the old configuration to the newly obtained configuration and W is a random number within [0,1], is then used to determine whether the trial configuration is acceptable. The acceptance rate of configurations generated in this way is found to range from 0.35 to 0.5.

The initial configuration is constructed from the zeroth generation in a generation-wise manner. To facilitate this process, we fix the distance between two bonded beads to be unity and allow partial overlapping between nonbonded beads. Additional conditions are also imposed: the angle between the two neighboring

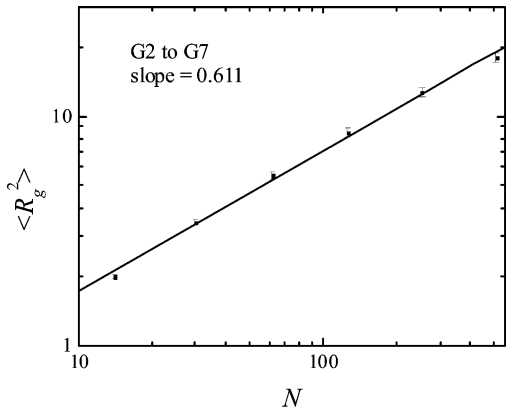

Figure 2. Mean-square radius of gyration of a dendrimer as a function of the total number of beads.

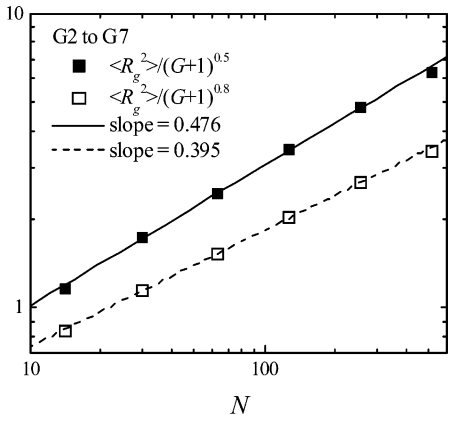

Figure 3. Variations of $\langle R_g^2 \rangle/(G+1)^{1/2}$ and $\langle R_g^2 \rangle/(G+1)^{4/5}$ with the total number of beads of a dendrimer.

bonds on a branching point leading to a same generation is randomly specified with 120°, while the angle between two bonds leading to different generations falls between 120° and 180°. The attached polymer chain on each terminal bead of the dendrimer is generated by successively adding the chain beads outward to avoid penetration into the dendrimer. For most of the cases, 10^6 MC steps are applied for equilibration, which has been ensured by monitoring the system energy. In the next 10^6 MC steps, a realization is taken for every 10^3 steps. 1000 independent runs are conducted, and average quantities are calculated on the basis of an ensemble of 10^6 configurations. For the case of $G = 6$ and $N_{\text{chain}} = 9$ (i.e., $N_{\text{total}} = 1406$), 5×10^6 MC steps are used for equilibration, followed by 5×10^6 MC steps, from which a realization is taken for every 2×10^3 steps. 100 independent runs are carried out.

3. Results and Discussion

a. Structural Properties of Dendrimer without Polymer Attachment. A quantitative estimate of the dendrimer size can be given by the mean-square radius of gyration:

$$\langle R_g^2 \rangle = \frac{1}{N} \langle \sum_{i=1}^{N} (\mathbf{r}_i - \mathbf{r}_C)^2 \rangle \tag{6}$$

where $\mathbf{r}_i$ is the position of bead i and $\mathbf{r}_C$ is the center of mass of the dendrimer. Figure 2 shows the dependence of $\langle R_g^2 \rangle$ on N in a double-logarithmic plot. Note that the error bars are small for all the results presented in this paper. To demonstrate, we only show the error bars in Figure 2. The best linear fit in Figure 2 has a slope of 0.611, which is close to 0.59 from Neelov and Adolf's simulation of the same model, except an additional core bead,[24] and to 0.59−0.62 obtained by those[17,27] using the other architecture mentioned in the Introduction. There existed a controversy of whether the solvent quality affects the scaling behavior of dendrimers until recent works[23,35] found that with a fixed spacer length, $\langle R_g^2 \rangle$, scales as $N^{2/5}(G+1)^{4/5}$, $N^{1/2}(G+1)^{1/2}$, and $N^{2/3}$ for the good, Θ, and poor solvents, respectively. Expressing G in terms of N using eq 3, one can easily find that $N^{2/5}(G+1)^{4/5}$, $N^{1/2}(G+1)^{1/2}$, and $N^{2/3}$ can hardly be distinguished for not so large N as used in many of simulation works. It also means that a power law does not really apply for good and Θ solvent conditions as $G \sim \ln N$. To demonstrate this, we replot the simulation results in Figure 2 by $\langle R_g^2 \rangle/(G+1)^{1/2}$ and $\langle R_g^2 \rangle/(G+1)^{4/5}$ vs N in Figure 3 and find that the linear fits also appear good for both with slopes equal to 0.476 and 0.395, respectively. It should be remembered that the values of parameters used in our simulations correspond to a state near the Θ condition.

The dendrimer dynamic size can be reflected by the hydrodynamic radius R_h, which can be measured experimentally by, for instance, dynamic light scattering, and is related to the long-time diffusivity D of the dendrimer through the Einstein−Stokes equation

$$D = \frac{k_B T}{6\pi\mu R_h} \tag{7}$$

where μ is the viscosity of the solvent. For a neutral linear chain of length N_P, D can hardly be distinguished from the Kirkwood short-time diffusivity[38] defined as[39]

$$D^K = \frac{D_0}{N_p} + \frac{k_B T}{6\pi\mu} \left\langle \frac{1}{R_{ij}} \right\rangle \tag{8}$$

with

$$\left\langle \frac{1}{R_{ij}} \right\rangle = \frac{1}{N_p^2} \sum_{i \neq j} \left\langle \frac{1}{|\mathbf{r}_i - \mathbf{r}_j|} \right\rangle \tag{9}$$

based on the Rotne−Prager−Yamakawa hydrodynamic interaction tensor. It can be easily proved that the above expression is also applicable to a dendrimer ($N_p = N$) or a dendrimer−polymer conjugate ($N_p = N_{\text{total}}$). Since a dendrimer is less flexible than a linear polymer, it is reasonable to hypothesize $D \approx D^K$, and R_h can then be determined using eqs 7−9. The log−log plot of R_h against N shown in Figure 4 exhibits a linear relation with a slope of 0.318, which is close to the scaling exponent of $\langle R_g^2 \rangle^{1/2}$. The diffusivity of the dendrimer is proportional to $N^{-0.318}$, similar to the recent reported result $D \sim N^{-0.35}$ from the calculation of mean-square displacement of mass center by Brownian dynamics simulations.[28]

A dendrimer's internal structure can be represented by the radial bead distribution function $\rho(r)$ with $r = 0$ being its center of mass, given by

$$\rho(r) = \frac{H(r)}{dV} \tag{10}$$

where $H(r)$ is the number of beads falling in the a spherical shell region between r and $r + \delta r$ with volume

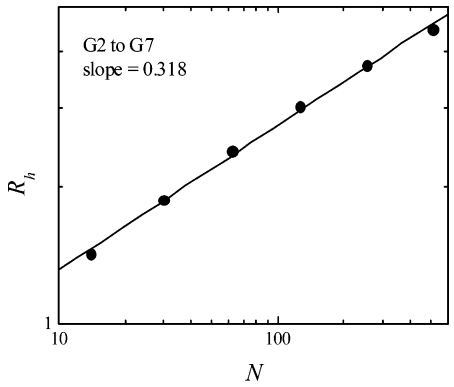

Figure 4. Average hydrodynamic radius of a dendrimer as a function of the total number of beads.

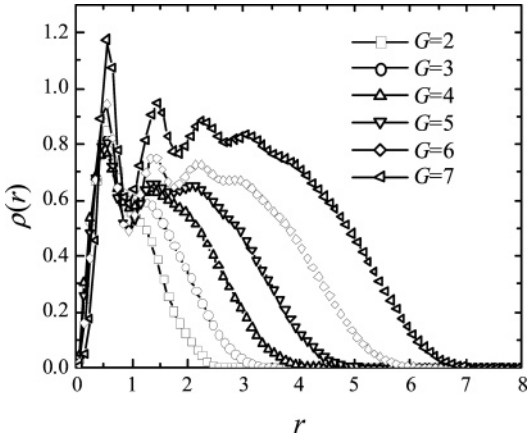

Figure 5. Radial distribution function of dendrimer beads for different generations.

dV. The shell bin thickness δr is set to be 0.1 in our simulation. Figure 5 shows the bead distribution for dendrimers of various generations. It can be seen that the multipeak behavior of the distribution becomes more pronounced as G increases, and the number of peaks is smaller than $G + 1$. Also, $\rho(r)$ becomes a monotonic decreasing function at large r and can span a considerable range. This behavior indicates that a dendrimer of more generations possesses a more ordered structure for the interior part. It has been reported in the literature[17,22,26,28−30] that outer branches in a dendrimer can fold back and penetrate into the interior part. Such a behavior can be inferred from the radial distribution function of terminal beads $\rho_{end}(r)$ shown in Figure 6. It can be found that the distribution becomes quite broad and uniform for $G = 6$ and 7, spanning approximately from $r = 1$ (inner) to 5 (outer). Evidently, the terminal beads can be located in the interior region of the dendrimer.

b. Structural Properties of Dendrimer−Polymer Conjugate. To determine the size of a dendrimer−polymer conjugate, we calculate the mean-square radius of gyration of the conjugate

$$\langle R_{g,conj}{}^2\rangle = \frac{1}{N_{total}}\langle \sum_{i=1}^{N_{total}} (\mathbf{r}_i - \mathbf{r}_{C,conj})^2\rangle \qquad (11)$$

where $\mathbf{r}_{C,conj}$ is the center of mass of the conjugate. Figure 7 plots $\langle R_{g,conj}{}^2\rangle$ against N_{total} for a G3 dendrimer with 16 linear chains grafted to its terminal beads. As expected, the conjugate increases in size with the length of attached chains. The dependence of $\langle R_{g,conj}{}^2\rangle$ on N_{total}

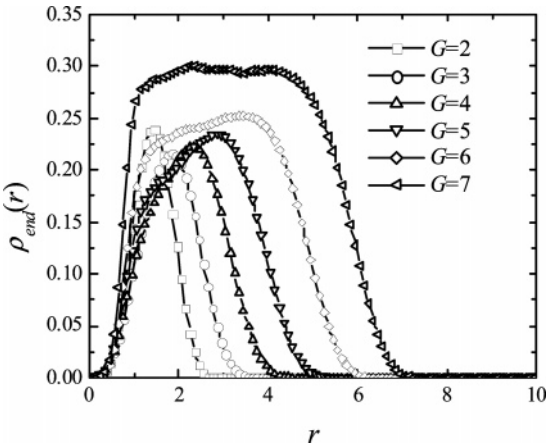

Figure 6. Radial distribution function of the end beads of a dendrimer for different generations.

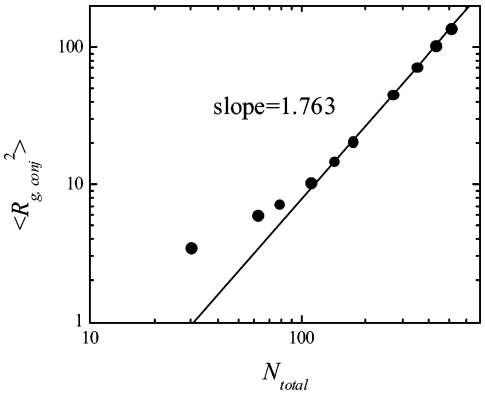

Figure 7. Mean-square radius of gyration of a G3 conjugate as a function of the total number of beads.

does not follow a simple power law. However, a linear relationship seems to emerge in the log−log plot for $N_{total} \geq 174$ (i.e., $N_{chain} \geq 9$). When long chains are attached, the size of dendrimer moiety becomes small as compared with that of the whole conjugate. For example, $\langle R_{g,conj}{}^2\rangle$ at $N_{chain} = 9$ is found to be 5.95 times larger than $\langle R_g{}^2\rangle$ of the dendrimer moiety in the core. Therefore, the contribution from the attached polymers becomes comparatively important. The slope of the fitting line 1.763 indicates that the conjugate structure is less compact than an unmodified dendrimer owing to the attachment of polymer chains. The conformation of the grafted polymer will be analyzed later in detail.

Kojima et al.[7] experimentally found that PAMAM with attached M-PEG had a stronger ability to encapsulate anticancer drugs and speculated a larger interior space in such PAMAM. To verify their conjecture, we plot $\langle R_g{}^2\rangle$ of the core dendrimer determined from eq 1 against N_{chain} for a G3 conjugate in Figure 8. Also shown in the figure is $\langle R_{g,end}{}^2\rangle$, which takes into account only the terminal beads of the dendrimer. It can be clearly seen that $\langle R_g{}^2\rangle$ and $\langle R_{g,end}{}^2\rangle$ both increase with the length of attached chains and then gradually approach constant values around 5 and 6.8, respectively. Because of the additional steric effect imposed by the attachment, the end beads of the dendrimer moiety are repelled to its outer region, as compared to the end beads of a dendrimer without grafted chains, which can stay in a more inner region. As a result, the repelling of the end beads makes the core dendrimer more extended as shown in Figure 8. It can also be seen that the increase of $\langle R_{g,end}{}^2\rangle$ with N_{chain} is more appreciable than that of

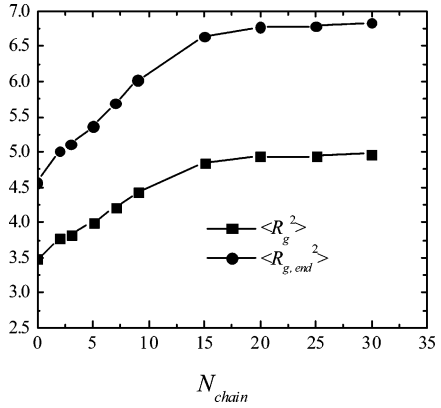

Figure 8. Variation of $\langle R_g^2 \rangle$ and $\langle R_{g,end}^2 \rangle$ with the length of attached chains for a G3 conjugate.

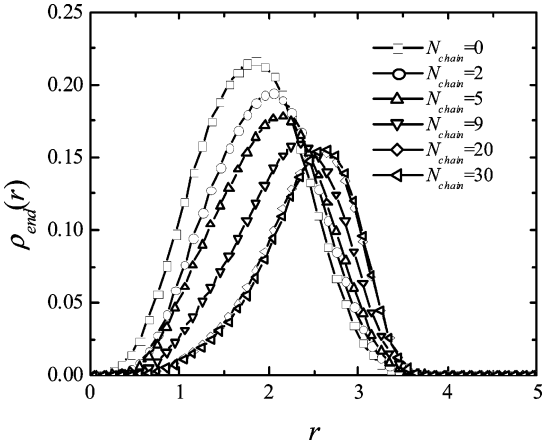

Figure 9. Radial distribution function of the end beads of a G3 conjugate for different lengths of attached chains.

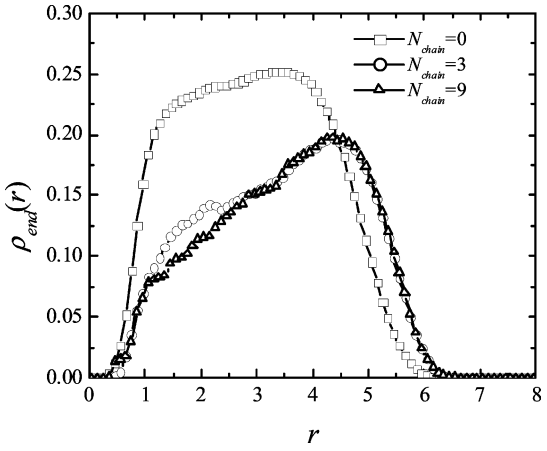

Figure 10. Radial distribution function of the end beads of a G6 conjugate for different lengths of attached chains.

$\langle R_g^2 \rangle$. When the length of attached chains becomes large enough, the size of core dendrimer no longer increases, although the conjugate can still increase in size as shown in Figure 7.

The distribution function of the end beads for a G3 conjugate is shown in Figure 9. We find that the peak of $\rho_{end}(r)$ shifts to a larger r for a larger N_{chain}, but the distribution functions become almost indiscernible for $N_{chain} \geq 20$, consistent with the trend shown in Figure 8. These results provide a further evidence for the repelling of end beads to the outer area. A similar plot for a G6 conjugate is presented in Figure 10. It can be seen that not only does the distribution function shift

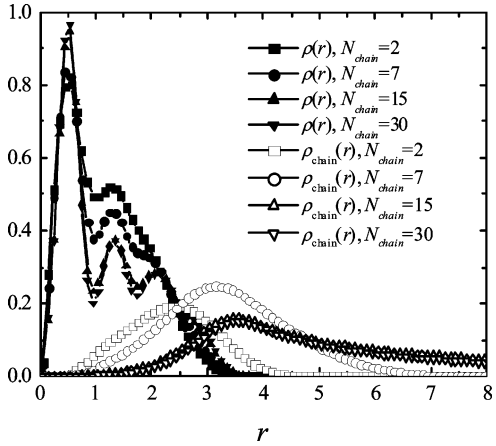

Figure 11. Radial distribution function of dendrimer beads and of polymer beads in a G3 conjugate for different lengths of attached chains.

to large r, but also the distribution becomes less broad and uniform. This behavior indicates that it is difficult for the end beads to considerably fold back because of the steric effect inducted by the grafted chains. As such, a more ordered structure is expected in the core dendrimer. Figure 11 shows the distributions of the dendrimer beads and the polymers beads for a G3 conjugate. It can be seen that the multipeak behavior becomes more pronounced for the distribution of dendrimer beads when the length of the attached chains is increased. The distribution function of dendrimer beads indeed becomes indiscernible for $N_{chain} \geq 15$. This result once again confirms the saturation of dendrimer size increase for a large enough length of attached chains as shown in Figure 8. One can also find from Figure 11 that the beads of the attached polymers are located at larger r for longer chains. It should be pointed out that $\rho_{chain}(r)$ for $N_{chain} = 30$ becomes larger when $r > 9$ and has a longer tail than that for $N_{chain} = 15$, although they appear quite similar in the r range shown in Figure 11. Moreover, the overlapping of the bead distribution functions for the dendrimer and the attached chains implies nonexistence of a clear boundary between the core dendrimer and the shell polymer in the conjugate.

Since the presence of grafted polymers can enlarge the dendrimer moiety, it is interesting to investigate how the attachment affects the shape of the dendrimer in a conjugate. The instantaneous shape of a dendrimer can be represented by the three eigenvalues E_1, E_2, and E_3 (in descending order) of the moment of inertia tensor defined as

$$\mathbf{E} = \frac{1}{N}\sum_{i=1}^{N}(\mathbf{r}_i - \mathbf{r}_C)(\mathbf{r}_i - \mathbf{r}_C) \qquad (12)$$

The square roots of $\langle E_1 \rangle$, $\langle E_2 \rangle$, and $\langle E_3 \rangle$ are the characteristic lengths of the three principal axes for the average shape. Figure 12 shows the variations of the eigenvalue ratios with the length of attached polymers for a G3 conjugate. Without polymer attachment, a dendrimer has $\langle E_1 \rangle$:$\langle E_2 \rangle$:$\langle E_3 \rangle$ = 3.10:1.84:1 as opposed to 16.0:3.24:1 for a linear polymer,[40] indicating that a dendrimer is shaped like an ellipsoid with three comparable axis lengths (1.76:1.36:1). When linear polymers are attached to the terminal beads of a dendrimer, $\langle E_1 \rangle / \langle E_3 \rangle$ and $\langle E_2 \rangle / \langle E_3 \rangle$ increase significantly with N_{chain} and then level off respectively to 5.9 and 3.2 for $N_{chain} \geq 15$,

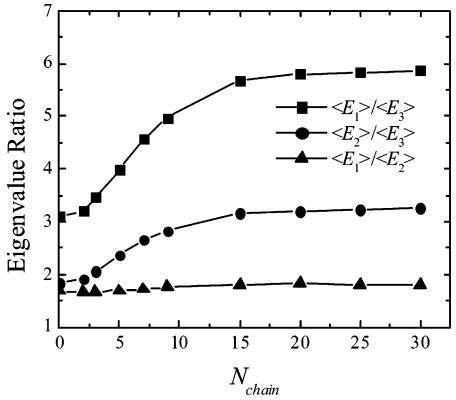

Figure 12. Variation of the eigenvalue ratios of the dendrimer core in a G3 conjugate with the length of attached chains.

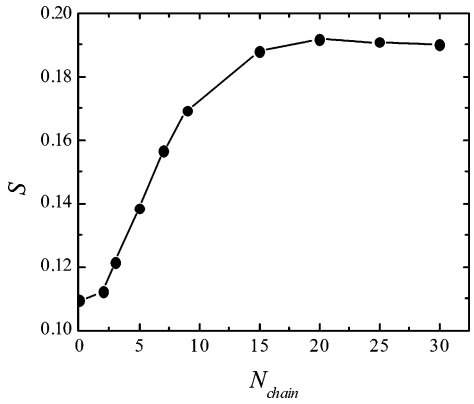

Figure 13. Variation of the asphericity of the dendrimer core in a G3 conjugate with the length of attached chains.

whereas $\langle E_1\rangle/\langle E_2\rangle$ only increases slightly from 1.7 to 1.8. These results reveal that the attachment causes the dendrimer to become more anisotropic than the aforementioned ellipsoid. To determine the shape deviation of the dendrimer from a sphere, we calculate the asphericity defined as[29]

$$S = 1 - 3\langle B\rangle/\langle A^2\rangle \tag{13}$$

where

$$A = E_1 + E_2 + E_3$$

$$B = E_1E_2 + E_2E_3 + E_3E_1$$

Note that $S = 0$ indicates a sphere. Figure 13 plots S against N_{chain} for a G3 conjugate, clearly showing that the core dendrimer deviates more in shape from a sphere in the presence of the attached polymers. Maiti et al.[29] have reported that the asphericity of a dendrimer without grafted chains decreases with generation up to G6. The more spherical conformation for a higher generation can be attributed to a higher degree of back-folding, as shown in Figure 6. With grafted chains, Figures 9 and 10 have shown the reduced back-folding with increasing chain length, which can therefore account for the increased asphericity.

As mentioned earlier, a considerable steric effect exists between the beads of the attached polymers and the dendrimer moiety. The conformation of the grafted chains is expected to be different from that of a corresponding free polymer. We plot in Figure 14 the mean-square end-to-end distance of the attached polymers $\langle R_{\text{ete}}^2\rangle$ against $(N_{\text{chain}} - 1)$ for a G3 conjugate. The

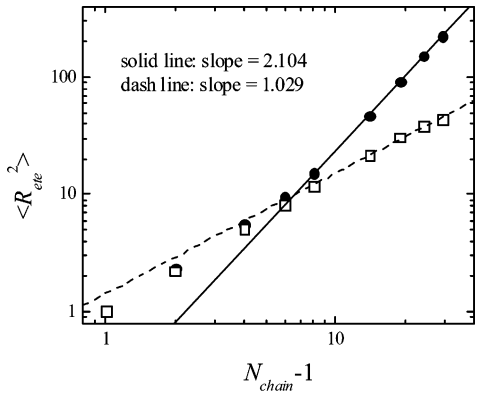

Figure 14. Mean-square end-to-end distance of the attached chains (circles) in a G3 conjugate as a function of the chain length. The results of a corresponding free chain (squares) are also shown.

corresponding results of a free chain are also shown in the figure for comparison. To examine the scaling behavior, we exclude the results of very short chains. The solid line in Figure 14 is a linear fit of the results for attached chains of $N_{\text{chain}} \geq 9$, while the dashed line is a corresponding fit for the free polymer of $N_{\text{chain}} \geq 9$. As can be seen, the slope of the latter, 1.029, clearly indicates a good agreement with the known power law for a free, coiled chain in the near Θ condition. The polymers attached to a G3 dendrimer, in contrast, show a stronger dependence on the chain length with the exponent equal to 2.104. This value implies that the attached chains are quite elongated due to volume exclusion and indeed have become brushlike. It can also be found from the figure that the end-to-end distance of short grafted polymers ($N_{\text{chain}} < 9$) obviously has a weaker dependence on the chain length as compared to the behavior of longer chains. To the contrary, a free short chain appears to nearly follow the same power law as its long counterpart. This difference indicates that when the attached polymers are long enough, they cannot find a sufficient space to accommodate themselves and thus cannot confomationally behave as free coiled chains, owing to the nearby beads of the neighboring chains and of the dendrimer. Despite the steric constraint, back-folding of the end beads of the dendrimer moiety can still take place, but to a lesser extent, as can be seen from Figures 9 and 10, where the breadth of the end bead distribution remains noticeable.

Despite no sharp border between the core dendrimer and the polymer attachment, it is desirable to estimate an effective thickness of the "polymer shell". Here, we define two effective shell thicknesses as

$$d_1 = \langle R_{\text{g,conj}}^2\rangle^{1/2} - \langle R_{\text{g}}^2\rangle^{1/2} \tag{14}$$

$$d_2 = \langle R_{\text{end,conj}}^2\rangle^{1/2} - \langle R_{\text{end}}^2\rangle^{1/2} \tag{15}$$

where $R_{\text{end,conj}}$ is the radius of gyration of terminal beads of the attached polymers in the conjugate. Figure 15 plots d_1 and d_2 against N_{chain} logarithmically for a G3 conjugate. The dashed and the solid line are the linear fits of the results for $N_{\text{chain}} \geq 9$. Both slopes are close to unity, indicating that the shell thickness grows linearly with the attached chain length for long enough grafted polymers. This behavior is consistent with that of end-to-end distance of the attached polymer shown in Figure 14. Note that the value of d_2 is indeed closer to $\langle R_{\text{ete}}^2\rangle^{1/2}$ than d_1. It is also interesting to observe that the chain

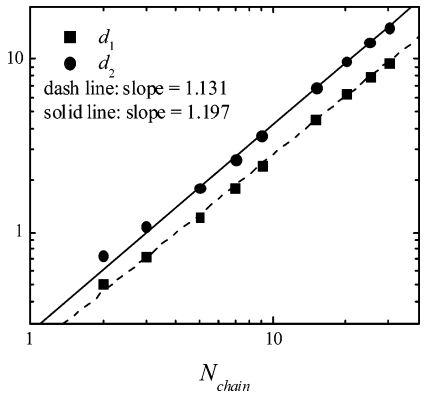

Figure 15. Effective shell thickness of a G3 dendrimer−polymer conjugate as a function of the length of attached chains.

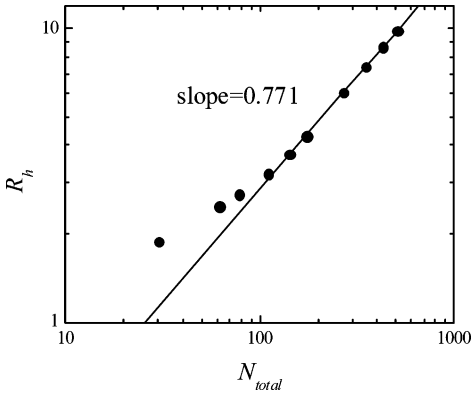

Figure 16. Average hydrodynamic radius of a G3 conjugate as a function of the total number of beads.

length dependence of the effective shell thickness for shorter chains does not differ very much from that for longer chains. Since there is no clear boundary between the dendrimer moiety and the attachment, the shell thickness defined in eq 14 or 15 cannot be equivalently represented by the end-to-end distance. This may also justify why the exponents shown in Figure 15 exceed unity.

An experimental method to study the effect of polymer attachment is a measurement of conjugate diffusivity, for instance, by dynamic light scattering. It is therefore essential to examine how the hydrodynamic radius is affected by the chain attachment. Figure 16 shows the variation of the hydrodynamic radius of a G3 conjugate with N_{total}. We find that when the beads of the attached chains greatly outnumber the dendrimer beads, the hydrodynamic radius appears to scale as $N_{\text{total}}^{0.771}$. The exponent is close to 0.88 for the gyration radius of the conjugate. Our simulation results of end-to-end distance of attached polymers have shown a brushlike behavior. For a free brushlike chain with length N_{chain}, its hydrodynamic radius is proportional to $N_{\text{chain}}/\ln N_{\text{chain}}$.[41] To verify the hydrodynamic behavior of attached chains, we calculate their average hydrodynamic radius and present the results in Figure 17 for a G3 conjugate. The brushlike hydrodynamic behavior can be clearly seen.

Finally, we compare our simulation results with available experimental data for dendrimer−polymer conjugates. Kojima et al.[7] used a size-exclusion chromatography column calibrated with PEG standards and applied the equation developed by Hester and Mitchell[42] to estimate the hydrodynamic radii of dendrimers and conjugates. The values are found to be 3.5, 6.4, and 12.5

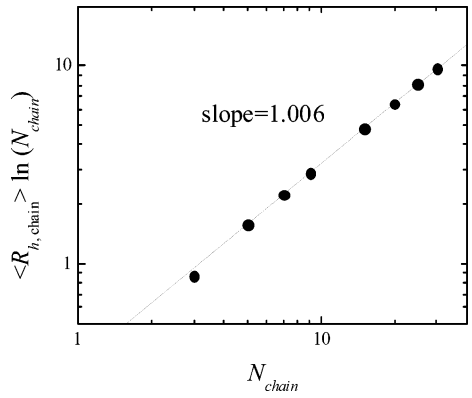

Figure 17. Chain length dependence of hydrodynamics radius of the attached polymers in a G3 conjugate.

nm for G3-PAMAM, M-PEG(550)-G3-PAMAM, and M-PEG(2000)-G3-PAMAM, respectively, and accordingly the corresponding ratio is 1:1.83:3.57. To make a crude comparison, we regard every seven bonds connecting two neighboring amino groups in PAMAM as a unit segment length l_0, and hence PEG(550) and PEG(2000) can be approximately represented by linear chains of 5 beads and 20 beads, respectively. The corresponding hydrodynamic radii from our simulation yield a ratio of 1:1.70:3.95, which is in acceptable agreement with Kojima's estimate.

4. Conclusion

MC simulations of dendrimers of generations $G = 2-7$ and dendrimer−polymer conjugates in near Θ condition have been carried out based on a bead−spring model. The dependence of the mean-square radius of gyrations of the dendrimer on the total number of beads is well fitted by a power law with an exponent of 0.611. Dendrimers of higher generations possess a more ordered structure for the interior region, and their end beads can fold back to stay in the inner part. All these behaviors are in agreement with those reported in the literature. We have also calculated the hydrodynamic radius of the dendrimer based on the Kirkwood diffusivity and arrived at a scaling behavior $N^{-0.318}$, which is similar to $N^{-0.35}$ inferred from the long-time diffusivity by BD simulations.

For dendrimer−polymer conjugates, our simulations have found that the polymer attachment can expand the dendrimer moiety in the core of the conjugate and also lead to a more ordered structure. Back-folding of the terminal segments of the dendrimer is reduced because of the additional steric effect imposed by the grafted polymers. Therefore, the periphery of the dendrimer becomes dense as compared to its unmodified counterpart. However, there exists no clear boundary between the core dendrimer and the attachment shell. The effect of attachment on the dendrimer structural behavior is found to increase with the length of attached chains but become saturated for long enough polymers. The expansion of the dendrimer moiety produces more free space inside and can thus enhance drug encapsulation in principle. When the grafted polymers are long enough, the substantial steric effect renders the chains brushlike, as inferred from the scaling behavior of their end-to-end distance and hydrodynamic radius. The effective thickness of the attachment shell shows a similar scaling behavior to the end-to-end distance of grafted polymers. We have also found that the hydrodynamic

radius of the conjugate with fixed generations appears to follow a power law with exponent of 0.771 when the grafted chains become sufficiently long. This scaling behavior can in principle be tested experimentally by measuring the diffusivity of conjugates with varying molecular weights of grafted polymers. A comparison of our simulation result with the limited experimental data available in the literature has indeed shown certain agreement.

Acknowledgment. The authors are grateful to the financial support by National University of Singapore through Grant R-279-000-172-112.

References and Notes

(1) Bosman, A. W.; Janssen, H. M.; Meijer, E. W. *Chem. Rev.* **1999**, *99*, 1665.
(2) Aulenta, F.; Hayes, W.; Rannard, S. *Eur. Polym. J.* **2003**, *39*, 1741.
(3) Boas, U.; Heegaard, P. M. H. *Chem. Soc. Rev.* **2004**, *33*, 43.
(4) Jansen, J. F. G. A.; de Brabander-van den Berg, E. M. M.; Meijer, E. W. *Science* **1994**, *266*, 1226.
(5) Jansen, J. F. G. A.; Meijer, E. W. *J. Am. Chem. Soc.* **1995**, *117*, 4417.
(6) Zhuo, R. X.; Du, B.; Lu, Z. R. *J. Controlled Release* **1999**, *57*, 249.
(7) Kojima, C.; Kono, K.; Maruyama, K.; Takagishi, T. *Bioconjug. Chem.* **2000**, *11*, 910.
(8) Rittner, K.; Benavente, A.; Bompard, S,; Heitz, F.; Divita, G.; Brasseur, R.; Jacobs, E. *Mol. Therapy* **2002**, *5*, 104.
(9) Roberts, J. C.; Bhalgat, M. K.; Zera, R. T. *J. Biomed. Mater. Res.* **1996**, *30*, 53.
(10) Malik, N.; Wiwattanapatapee, R.; Klopsch, R.; Lorenz, K.; Frey, H.; Weener, J. W.; Meijer, E. W.; Paulus, W.; Duncan, R. *J. Controlled Release* **2000**, *65*, 133.
(11) Liu, M.; Kono, K.; Fréchet, J. M. J. *J. Polym. Sci., Part A: Polym. Chem. Ed.* **1999**, *37*, 3492.
(12) de Gennes, P.-G.; Hervet, H. *J. Phys., Lett.* **1983**, *44*, L351.
(13) Rosenfeldt, S.; Dingenouts, N.; Ballauff, M.; Werner, N.; Vogtle, F.; Lindner, P. *Macromolecules* **2002**, *35*, 8098.
(14) Topp, A.; Bauer, B. J.; Tomalia, D. A.; Amis, E. J. *Macromolecules* **1999**, *32*, 7232.
(15) Prosa, T. J.; Bauer, B. J.; Amis, E. J. *Macromolecules* **2001**, *34*, 4897.
(16) Rey, A.; Freire, J. J.; de la Torre, J. G. *Macromolecules* **1987**, *20*, 2385.
(17) Murat, M.; Grest, S. *Macromolecules* **1996**, *29*, 1278.
(18) Mazo, M. A.; Zhilin, P. A.; Gusarova, E. B.; Sheiko, S. S.; Balabaev, N. K. *J. Mol. Liq.* **1999**, *82*, 105.
(19) Chen, Z. Y.; Cai, C. *Macromolecules* **1999**, *32*, 5423.
(20) Welch, P.; Muthukumar, M. *Macromolecules* **1998**, *31*, 5892.
(21) Welch, P.; Muthukumar, M. *Macromolecules* **2000**, *33*, 6159.
(22) Karatasos, K.; Adolf, D. B.; Davies, G. R. *J. Chem. Phys.* **2001**, *115*, 5310.
(23) Sheng, Y.-J.; Jiang, S.; Tsao, H.-K. *Macromolecules* **2002**, *35*, 7865.
(24) Neelov, I. M.; Adolf, D. B. *Macromolecules* **2003**, *36*, 6914.
(25) Harreis, H. M.; Likos, C. N.; Ballauff, M. *J. Chem. Phys.* **2003**, *118*, 1979.
(26) Götze, I. O.; Harreis, H. M.; Likos, C. N. *J. Chem. Phys.* **2004**, *120*, 7761.
(27) Lyulin, S. V.; Evers, L. J.; van der Schoot, P.; Darinskii, A. A.; Lyulin; A. V. Michels, M. A. J. *Macromolecules* **2004**, *37*, 3049.
(28) Lyulin, S. V.; Darinskii, A. A.; Lyulin, A. V.; Michels, M. A. J. *Macromolecules* **2004**, *37*, 4676.
(29) Maiti, P. K.; Cağin, T.; Wang, G.; Goddard, W. A. *Macromolecules* **2004**, *37*, 6236.
(30) Maiti, P. K.; Cağin, T.; Wang, Lin, S.-T.; G.; Goddard, W. A. *Macromolecules* **2005**, *38*, 979.
(31) Bosko, J. T.; Todd, B. D.; Sadus, R. J. *J. Chem. Phys.* **2004**, *121*, 12050.
(32) Götze, I. O.; Likos, C. N. *Macromolecules* **2003**, *36*, 8189.
(33) Chen, Z. Y.; Cai, C. *Macromolecules* **1997**, *30*, 5104.
(34) Timoshenko, E. G.; Kuznetsov, Y. A.; Connolly, R. *J. Chem. Phys.* **2002**, *117*, 9050.
(35) Giupponi, G.; Buzza, D. M. A. *J. Chem. Phys.* **2004**, *120*, 10290.
(36) Kolhe, P.; Misra, E.; Kannan, R. K.; Kannan, S.; Lieh-L, M. *Int. J. Pharm.* **2003**, *259*, 143.
(37) Allen, M. P.; Tildesley, D. J. *Computer Simulation of Liquids*; Clarendon: Oxford, 1987.
(38) Liu, B.; Dünweg, B. *J. Chem. Phys.* **2003**, *118*, 8061.
(39) Kirkwood, G. *J. Polym. Sci.* **1953**, *12*, 1.
(40) Ceperley, D.; Kalos, M. H.; Lebowitz, J. L. *Macromolecules* **1981**, *14*, 1472.
(41) Doi, M.; Edwards, S. F. *The Theory of Polymer Dynamics*; Clarendon: Oxford, 1986.
(42) Hester, R. D.; Mitchell, P. H. *J. Polym. Sci., Chem. Ed.* **1980**, *18*, 1727.

MA050997W